Squeezing properties of a two-transverse-mode degenerate optical parametric oscillator with an injected signal

Carlos Navarrete-Benlloch, Eugenio Roldán, and Germán J. de Valcárcel
Departament d'Òptica, Universitat de València, Carrer del Doctor Moliner 50, E-46100 Burjassot, Spain
(Received 29 July 2010; published 12 April 2011)

We study the classical and quantum properties of a degenerate optical parametric oscillator (DOPO) tuned to the first family of transverse modes at the down-converted frequency, under the injection of a resonant TEM_{10} mode. Unlike the usual single-mode DOPO with injected signal, large levels of squeezing are predicted even for relatively large injections. We interpret these results in connection with the spontaneous symmetry breaking predicted for this system in the absence of injection and with the existence of a bifurcation giving rise to the switching on of the (noninjected) TEM_{01} mode.

DOI: 10.1103/PhysRevA.83.043812 PACS number(s): 42.50.Dv, 42.50.Lc, 42.50.Tx, 42.65.Yj

I. INTRODUCTION

Optical parametric oscillators (OPOs) are among the best sources of squeezed [1–4], correlated [5], and entangled [6] states of light in the so-called continuous-variable regime [7,8], which find applications in demanding areas such as high-precision metrology [9–11] or quantum information [12–14]. Especially relevant are frequency-degenerate OPOs (or DOPOs): In a DOPO a coherent light beam of frequency $2\omega_0$ pumps the resonator and is down-converted, through a nonlinear $\chi^{(2)}$ crystal placed inside the cavity, into another light beam at the subharmonic frequency ω_0, called signal beam.

It has been recently shown that the remarkable quantum properties of DOPOs are improved when multimode operation is considered: Both multilongitudinal modes DOPOs [15,16] and multitransverse modes DOPOs [17–20] exhibit more flexible and less critical quantum properties than the usual single-mode DOPO.

In this article we focus on a two-transverse-mode DOPO (2DOPO), which has been shown recently to exhibit quite interesting quantum properties [21,22]. A 2DOPO is pumped, as usual, by a Gaussian beam, but the cavity is tuned in such a way that, at the subharmonic frequency ω_0, it is not the fundamental (Gaussian) beam that resonates, but the modes belonging to the first transverse-mode family. Such family is composed of two Laguerre-Gaussian (LG) beams whose phase varies according to $e^{\pm i\phi}$, ϕ being the azimuth in the cavity transverse plane. Hence, these LG modes have well-defined orbital angular momentum (OAM) equal to $\pm\hbar$, as they are eigenmodes of the OAM operator $L_\phi = -i\hbar\partial_\phi$. As the interaction is parametric (the nonlinear crystal serves as a host, not gaining any net energy or momentum), energy and OAM conservation imply that any down-converted pump photon (having zero OAM and energy $2\hbar\omega_0$) will give rise to two signal photons of equal energy $\hbar\omega_0$ and opposite OAM. Hence, the 2DOPO is then a source of highly correlated photons carrying definite OAM [18]. A related phenomenon (the hyperentanglement between OAM and polarization degrees of freedom) has been predicted in (nondegenerate) OPOs tuned at transverse-mode families [23].

Hence, at the classical level, a 2DOPO above threshold emits an equally weighted linear superposition of the two LG modes, what is equivalent to the emission of a bright Hermite-Gauss (HG)—or TEM_{10}—mode [21,22]. The orientation of such TEM_{10} mode on the cavity transverse plane is not fixed, however, by the interaction, reflecting the rotational invariance of the system. It is this fact that is responsible for the outstanding properties of the 2DOPO: Quantum noise makes undetermined the emitted mode orientation, which allows for the complete determination (perfect squeezing) of its canonically conjugated momentum, which is the phase quadrature of the (dark) mode spatially crossed with respect to the bright one [22]. We can reword this in the following way: Above threshold a pattern is emitted that spontaneously breaks the rotational invariance of the system; quantum noise tends to restore this lost symmetry by making the pattern orientation fluctuate and become, in the long term, completely uncertain; finally, and allowed by Heisenberg's relation, a full certainty (perfect squeezing) of an observable is produced. As this mechanism (spontaneous symmetry breaking) occurs at any pump level above threshold, it is expected (and predicted [21,22]) that this quantum property is independent of that level, unlike usual single-mode DOPO squeezing that is (ideally) perfect only at DOPO threshold [24–27]. We note that similar behaviors happen in other nonlinear optical cavities in which a continuous symmetry is spontaneously broken above threshold [28–32]. Experimental evidence of such remarkable quantum properties have been recently reported [18–20].

The uncertainty in the orientation of the TEM_{10} mode emitted by a 2DOPO is inconvenient from the experimental viewpoint, as the local oscillator (LO) needed to perform the homodyning used to detect the quadrature squeezing must be matched to the emitted field. It is obvious, because of the quantum nature of the uncertainty, that by no means can any LO be matched to follow (instantaneously) the random rotation of the emitted field, and the deleterious effects of keeping the LO fixed during the detection process have been studied in [22]. Hence, some means of fixing this orientation is called for. Moreover, an injected signal at the subharmonic frequency is customarily used in experiments for stabilization and locking purposes. As the 2DOPO we are considering emits a HG (TEM_{10}) mode with arbitrary orientation in the absence of injection, we choose to inject a resonant TEM_{10} mode with fixed orientation and denote by 2DOPO-IS this injected 2DOPO. This injection breaks the rotational invariance of the system, and hence a degradation of the squeezing level is expected. The goal of this article is then to determine the

impact of the signal injection on the quantum properties of the 2DOPO.

Previously, we have considered the effect of imposing a symmetry breaking in a 2DOPO by using a simple toy model [21]: By assuming that the system has different cavity losses for the bright and dark modes, their orientation on the transverse plane is fixed and the problem of matching the dark mode with the LO is automatically resolved. In [21] we made such an estimate and concluded that the phenomenon is quite robust (the squeezing level was noncritical and still quite large). As well we have extended this simplified approach to the effect of an astigmatic resonator, which is a more realistic case [33].

As we show below, the 2DOPO-IS exhibits large levels of squeezing, larger than those exhibited by the usual single-mode DOPO with injected signal (1DOPO-IS), a result that is connected with the squeezing due to the spontaneous breaking of the rotational symmetry that exists in the absence of injection, but also to the existence of a new bifurcation in the system. This is the problem we treat in detail in the present article. Our work is closely related to that of Protsenko *et al.* [34], who considered a 1DOPO-IS (see also [35,36]). Indeed, our model contains, as a limit, the model studied in [34], but we shall see that the existence of a second signal mode substantially modifies the properties of the system.

The rest of the article is organized as follows. In Sec. II we present the model for the 2DOPO-IS, analyze its classical solutions and study their stability in Sec. III, and address the squeezing properties of the system in Sec. IV. Finally, in Sec. V we give our main conclusions.

II. MODEL

We consider an optical cavity of length L consisting of spherical mirrors, and containing a thin $\chi^{(2)}$ crystal. We assume that collinear, frequency-degenerate type-I phase matching occurs at the frequencies $2\omega_0$ (pump) and ω_0 (signal). The cavity is pumped by a coherent field of frequency $2\omega_0$ that is assumed to be matched to a fundamental cavity Gaussian mode, whose shape at the cavity waist plane reads

$$G(\mathbf{r}) = \sqrt{2/\pi}\, w_{\mathrm{p}}^{-1} \exp\left(-r^2/w_{\mathrm{p}}^2\right), \tag{1}$$

with $\mathbf{r}$ the transverse position vector and w_{p} the mode's radius [22]. Through a down-conversion process, light at frequency ω_0 is generated inside the cavity. In order to maximize the process a cavity resonance must exist at ω_0. We assume that the resonant mode at that frequency is not a fundamental Gaussian mode as usual, but the couple of modes forming a first transverse-mode family. In previous studies we used the LG basis,

$$L_{\pm 1}(\mathbf{r}) = (2/\sqrt{\pi}) w_{\mathrm{s}}^{-1} \exp\left(-r^2/w_{\mathrm{s}}^2\right)(r/w_{\mathrm{s}}) e^{\pm i\phi}, \tag{2}$$

where the expressions hold again at the cavity waist plane and we used polar coordinates (r,ϕ); w_{s} is the signal waist radius [22]. This basis is useful as it allows a clear picture of the interaction in terms of OAM conservation [17,21–23]. Alternatively, one can use the HG basis,

$$H_{\mu}(\mathbf{r}) = (2\sqrt{2/\pi}) w_{\mathrm{s}}^{-1} \exp\left(-r^2/w_{\mathrm{s}}^2\right)(\mu/w_{\mathrm{s}}), \tag{3}$$

$\mu = x,y$, which are usually called TEM_{10} and TEM_{01} modes. In (3) x and y are two arbitrary, orthogonal directions on the transverse plane; $\mathbf{r} = (x,y)$. The relation between LG and HG modes is given by

$$H_x(\mathbf{r}) = [L_{+1}(\mathbf{r}) + L_{-1}(\mathbf{r})]/\sqrt{2}, \tag{4a}$$

$$H_y(\mathbf{r}) = -i[L_{+1}(\mathbf{r}) - L_{-1}(\mathbf{r})]/\sqrt{2}. \tag{4b}$$

The HG basis is better adapted to our purposes here because, as stated in the Introduction, one of these modes is injected into the cavity at the signal frequency, and we choose it to be $H_x(\mathbf{r})$ for definiteness and without loss of generality.

At the resonator waist plane (where the nonlinear $\chi^{(2)}$ crystal is assumed to be placed), the interaction picture electric field can be written as $\hat{E}(\mathbf{r},t) = \hat{E}_{\mathrm{p}}(\mathbf{r},t) + \hat{E}_{\mathrm{s}}(\mathbf{r},t)$, where

$$\hat{E}_{\mathrm{p}}(\mathbf{r},t) = i\mathcal{F}_{\mathrm{p}} \hat{A}_{\mathrm{p}}(\mathbf{r},t) e^{-2i\omega_0 t} + \mathrm{H.c.}, \tag{5a}$$

$$\hat{E}_{\mathrm{s}}(\mathbf{r},t) = i\mathcal{F}_{\mathrm{s}} \hat{A}_{\mathrm{s}}(\mathbf{r},t) e^{-i\omega_0 t} + \mathrm{H.c.}, \tag{5b}$$

where $\mathcal{F}_{\mathrm{p}} = \sqrt{2}\mathcal{F}_{\mathrm{s}} = \sqrt{2\hbar\omega_0/\varepsilon_0 n L}$, n is the refractive index of the nonlinear crystal, and H.c. stands for Hermitian conjugate. The slowly varying envelopes are written as

$$\hat{A}_{\mathrm{p}}(\mathbf{r},t) = \hat{a}_0(t) G(\mathbf{r}), \tag{6a}$$

$$\hat{A}_{\mathrm{s}}(\mathbf{r},t) = \hat{a}_x(t) H_x(\mathbf{r}) + \hat{a}_y(t) H_y(\mathbf{r}). \tag{6b}$$

Alternatively, the signal field envelope can be expressed in the LG basis (2) [22] as

$$\hat{A}_{\mathrm{s}}(\mathbf{r},t) = \hat{a}_{+1}(t) L_{+1}(\mathbf{r}) + \hat{a}_{-1}(t) L_{-1}(\mathbf{r}), \tag{7}$$

with

$$\hat{a}_{\pm 1} = (\hat{a}_x \mp i\hat{a}_y)/\sqrt{2}, \tag{8}$$

according to (II). All boson operators $(\hat{a}_m, \hat{a}_m^{\dagger})$ verify standard, equal time commutation relations.

The Hamiltonian of the 2DOPO-IS reads

$$\hat{H} = i\hbar[\mathcal{E}_{\mathrm{p}} \hat{a}_0^{\dagger} + \mathcal{E}_{\mathrm{s}} \hat{a}_x^{\dagger} + \chi a_0 (\hat{a}_x^{\dagger 2} + \hat{a}_y^{\dagger 2})/2] + \mathrm{H.c.}, \tag{9}$$

where $\mathcal{E}_{\mathrm{p}}$ and $\mathcal{E}_{\mathrm{s}}$ are proportional to the complex amplitudes of the coherent, resonant beams at pump and signal frequencies, respectively, injected into the cavity (see the Appendix), and χ is proportional to the relevant nonlinear susceptibility (see [22] for an expression of χ in terms of physical parameters). With $\mathcal{E}_{\mathrm{s}} = 0$ Hamiltonian (9) describes a free-running 2DOPO and coincides with that considered previously by us [21,22] once relations (8) are used.

The problem is cast now in terms of the so-called positive P representation [37], in which boson operators $(\hat{a}_m, \hat{a}_m^{\dagger})$ are exactly mapped onto independent complex stochastic variables (α_m, α_m^{+}). Through the use of well-known techniques [37–39] a set of Langevin equations can be derived that governs the evolution of the α's. In our case we can use a short cut, leading to the same result: By borrowing Eqs. (10) from [22], using (8), and incorporating the signal injection similarly to the pump injection, the Langevin equations read [40]

$$\dot{\alpha}_0 = \mathcal{E}_{\mathrm{p}} - \gamma_{\mathrm{p}}\alpha_0 - \chi\left(\alpha_x^2 + \alpha_y^2\right)/2, \tag{10a}$$

$$\dot{\alpha}_x = \mathcal{E}_{\mathrm{s}} - \gamma_{\mathrm{s}}\alpha_x + \chi\alpha_0\alpha_x^{+} + \sqrt{\chi\alpha_0}\eta_x(t), \tag{10b}$$

$$\dot{\alpha}_y = -\gamma_{\mathrm{s}}\alpha_y + \chi\alpha_0\alpha_y^{+} + \sqrt{\chi\alpha_0}\eta_y(t), \tag{10c}$$

plus the equations for α_m^+ ($m = 0,x,y$), which are like those for α_m under the swapping $\alpha_m \longleftrightarrow \alpha_m^+$ and complex-conjugating complex quantities. Note that these equations incorporate cavity losses (γ_p is the cavity damping rate for the pump mode while γ_s is the common one to the signal fields: rotationally symmetric cavity). The real noises $\eta_m(t)$ are standard Gaussian white noises, having zero mean and nonzero correlations

$$\langle \eta_m(t)\eta_{m'}(t')\rangle = \delta_{m,m'}\delta(t-t'). \tag{11}$$

In the following we take $\mathcal{E}_\mathrm{p}$ as a positive real without loss of generality (this sets the phase of the pump laser as the reference phase), while $\mathcal{E}_\mathrm{s}$ can have a relative phase with respect to $\mathcal{E}_\mathrm{p}$.

In order to simplify the appearance of the above equations, we introduce

$$\tau = \gamma_\mathrm{s} t, \quad \beta_m = \frac{\chi}{\gamma_\mathrm{s}\sqrt{\gamma_\mathrm{p}/\gamma_m}}\alpha_m, \quad \zeta_m(\tau) = \frac{1}{\sqrt{\gamma_\mathrm{s}}}\eta_m(t), \tag{12}$$

where the new noises $\zeta_m(\tau)$ verify the usual statistical properties (11) in terms of the new dimensionless time τ. The Langevin equations read now

$$\dot\beta_0 = \kappa\left[\sigma - \beta_0 - \left(\beta_x^2+\beta_y^2\right)/2\right], \tag{13a}$$

$$\dot\beta_x = \varepsilon_\mathrm{i} - \beta_x + \beta_0\beta_x^+ + g\sqrt{\beta_0}\zeta_x(\tau), \tag{13b}$$

$$\dot\beta_y = -\beta_y + \beta_0\beta_y^+ + g\sqrt{\beta_0}\zeta_y(\tau), \tag{13c}$$

plus the equations for β_m^+. The derivative is with respect to the new dimensionless time τ. The above equations have only four free, dimensionless parameters,

$$\sigma = \frac{\chi\mathcal{E}_\mathrm{p}}{\gamma_\mathrm{p}\gamma_\mathrm{s}}, \quad \varepsilon_\mathrm{i} = \frac{\chi\mathcal{E}_\mathrm{s}}{\gamma_\mathrm{s}\sqrt{\gamma_\mathrm{p}\gamma_\mathrm{s}}}, \quad \kappa = \frac{\gamma_\mathrm{p}}{\gamma_\mathrm{s}}, \quad g = \frac{\chi}{\sqrt{\gamma_\mathrm{p}\gamma_\mathrm{s}}}. \tag{14}$$

These are, respectively, the normalized versions of the pump amplitude, the injected field amplitude (that is why the subscript "i"), the decay rate of the pumping field, and the nonlinear coupling coefficient. Model (13) is the one we study.

In the absence of injection, $\varepsilon_\mathrm{i} = 0$, model (13) describes a free-running 2DOPO and is equivalent to the model studied by us in [21,22]. In that case the 2DOPO threshold occurs at a pumping level $\sigma = 1$, which is a relevant value in the injected case as well, as we see in this paper.

III. CLASSICAL STEADY STATES AND THEIR STABILITY

From the quantum Langevin equations (II) the classical limit is recovered by neglecting the noise terms and by making the identification $\beta_m^+ \to \beta_m^*$ ($m = 0,x,y$),

$$\dot\beta_0 = \kappa\left[\sigma - \beta_0 - \left(\beta_x^2+\beta_y^2\right)/2\right], \tag{15a}$$

$$\dot\beta_x = \varepsilon_\mathrm{i} - \beta_x + \beta_0\beta_x^*, \tag{15b}$$

$$\dot\beta_y = -\beta_y + \beta_0\beta_y^*. \tag{15c}$$

In this section we study the steady states of this classical model, as well as their stability properties. Notice that by setting $\beta_y = 0$, Eqs. (15) become those for a 1DOPO-IS. Such model (generalized by the presence of detunings) was studied in [41] in the case of real ε_i and then extended to arbitrary injection phases in [34].

A straightforward inspection of (15) leads to the conclusion that for $\varepsilon_\mathrm{i} \neq 0$ there are only two types of classical solutions, either with $\beta_y = 0$ or with $\beta_y \neq 0$, both having $\beta_x \neq 0$. In the first case the intracavity signal field is single-mode and has the same shape as the injection; on the other hand, when $\beta_y \neq 0$ the intracavity field is in a coherent superposition of both transverse modes. We refer to these two types of states as the *one-mode* and *two-mode* solutions, respectively.

Steady states are obtained by setting to zero the time derivatives in (15). On the other hand, the study of the stability of such states against small perturbations is done via a usual linear stability analysis: The stability matrix $\mathcal{L}$, whose elements are given by $\mathcal{L}_{jk} = \partial\dot\beta_j/\partial\beta_k|_{\bar\beta}$ ($\bar\beta$ denotes variables at steady state), has a set of eigenvalues $\{\lambda_i\}_{i=1}^6$ and the studied solution is stable if all of them have a negative real part. The point at which $\mathrm{Re}\{\lambda_i\} = 0$ for some i marks a so-called bifurcation, indicating an instability.

In the following we decompose the fields into modulus and phase as

$$\varepsilon_\mathrm{i} = \sqrt{\mathcal{I}_\mathrm{i}}e^{i\varphi_\mathrm{i}}, \quad \beta_m = \sqrt{I_m}e^{i\varphi_m}, \tag{16}$$

when needed.

A. The one-mode solution

We look first for a solution in which the noninjected mode $H_y(\mathbf{r})$ is off ($\beta_y = 0$). This solution was the one analyzed in [34], and we refer to that work for the details. Using our notation, the intensity I_x of mode $H_x(\mathbf{r})$ verifies the implicit relation

$$\mathcal{I}_\mathrm{i} = \frac{2(\sigma^2 - X^2)^2(X-1)}{\sigma^2 + X^2 + 2\sigma X\cos 2\varphi_\mathrm{i}}, \tag{17}$$

where $X = 1 + \frac{1}{2}I_x$, which is a quintic polynomial in I_x, while its phase is given by

$$e^{i\varphi_x} = \pm\frac{\sigma e^{-i\varphi_\mathrm{i}} + Xe^{i\varphi_\mathrm{i}}}{\sqrt{\sigma^2 + X^2 + 2\sigma X\cos 2\varphi_\mathrm{i}}}, \tag{18}$$

where the plus and minus signs correspond, respectively, to cases $X > \sigma$ and $X < \sigma$. Finally, the intracavity pump field is given by

$$I_0 = \tfrac{1}{4}I_x^2 + \sigma^2 - \sigma I_x\cos 2\varphi_x, \tag{19a}$$

$$\varphi_0 = \arg\left(2\sigma - I_x e^{2i\varphi_x}\right). \tag{19b}$$

In Fig. 1 we show the dependence of the intensity I_x on the injected intensity $\mathcal{I}_\mathrm{i}$ in the case $\varphi_\mathrm{i} = 0$ (amplification regime) for various values of the pumping level σ as indicated. For $\sigma < 1$ (below the free-running 2DOPO threshold) the curve is single-valued, while for $\sigma > 1$ the curve is multivalued for small injection intensities. The location of the turning points (marked as TP1 and TP2) existing for $\sigma > 1$ can be obtained from Eq. (17) by solving $\partial\mathcal{I}_\mathrm{i}/\partial I_x = 0$ (see [34] for more details). One of them is analytical,

$$I_x^{\mathrm{TP1}} = 2(\sigma - 1), \tag{20}$$

which exists only if $\sigma > 1$, as expected. For $I_x = I_x^{\mathrm{TP1}}$, $\mathcal{I}_\mathrm{i} = 0$ as follows from (17), and then I_x^{TP1} corresponds to the upper turning points in Fig. 1. The intensity I_x^{TP2} at the lower turning points in Fig. 1 is given by a fourth-order polynomial, which we do not present here as it gives no analytical information

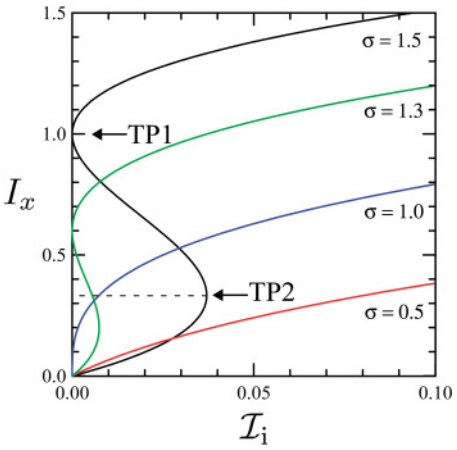

FIG. 1. (Color online) Intensity of the TEM_{10} mode for the "one-mode" solution as a function of the injected field intensity $\mathcal{I}_i$ for $\varphi_i = 0$ and the four indicated values of σ. Note that for $\sigma > 1$ the solution is three-valued. We have indicated the turning points TP1 and TP2 for the case $\sigma = 1.5$.

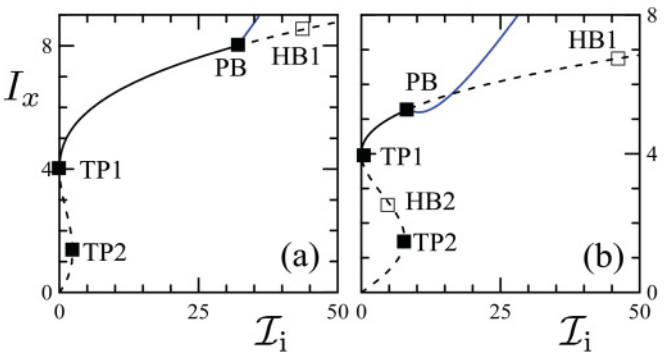

FIG. 2. (Color online) Steady states of the system on the plane $\langle \mathcal{I}_i, I_{10} \rangle$. Continuous and dashed lines correspond to stable and unstable solutions, respectively. The black and blue lines correspond to the "one-mode" and "two-modes" solutions, respectively. The parameter values are $\sigma = 3$ and $\varphi_i = 0, \kappa = 0.25$ in (a) and $\varphi_i = \pi/3$, $\kappa = 1$ in (b). Notice that for $\mathcal{I}_i \neq 0$ the pitchfork bifurcation where the TEM_{01} mode is switched on (marked as PB) is the only relevant bifurcation. TP1 and TP2 denote the turning points (see Fig. 1) and HB1 and HB2 denote two different Hopf bifurcations (which are always preceded by the bifurcations occurring at points TP1 and PB; see text).

and, moreover, because it plays no effective role in the system behavior, as is shown below.

The final conclusion is simple: For $\sigma < 1$ Eq. (17) has a single real and positive solution, while for $\sigma > 1$ the solution is three-valued for small injection intensities.

As for the stability of the one-mode solution, the stability matrix $\mathcal{L}$ turns out to be block-diagonal. One submatrix affects only the subspace (β_y, β_y^*) and then governs the possible switching-on of mode $H_y(\mathbf{r})$ (remember that in this one-mode solution $\beta_y = 0$), while the other affects the rest of variables and is the same one considered in [34]. Accordingly, the characteristic polynomial is factorized into two.

The first polynomial, quadratic in λ, governs the evolution of perturbations of the variables (β_y, β_y^*) as commented, and gives the following two eigenvalues

$$\lambda_{1,2} = -1 \pm \sqrt{I_0}, \tag{21}$$

with I_0 given by Eq. (19a). Solving $\lambda_1 = 0$ gives two solutions, namely, $I_x = I_x^{\mathrm{TP1}}$ [Eq. (20)], which occurs at $\mathcal{I}_i = 0$, and

$$I_x = 2\sqrt{1 + \sigma^2 + 2\sigma \cos 2\varphi_i} \equiv I_x^{\mathrm{PB}}, \tag{22}$$

which occurs at, using (17),

$$\mathcal{I}_i = 4(1 + \sigma \cos 2\varphi_i + \sqrt{1 + 2\sigma \cos 2\varphi_i + \sigma^2}) \equiv \mathcal{I}_i^{\mathrm{PB}}. \tag{23}$$

In a moment it will become clear why we denote by PB this new bifurcation.

As shown in Fig. 2, the analyzed solution is stable (i.e., $\lambda_1 < 0$) for $I_x^{\mathrm{TP1}} < I_x < I_x^{\mathrm{PB}}$. For $I_x > I_x^{\mathrm{PB}}$ or $I_x < I_x^{\mathrm{TP1}}$, $\lambda_1 > 0$ and the one-mode solution is unstable. For $\sigma < 1$ the turning points TP1 and TP2 do not exist and the one-mode solution is stable all along its unique branch until $I_x = I_x^{\mathrm{PB}}$. On the other hand, for $\sigma > 1$ the one-mode solution is stable only in the portion of its upper branch (Fig. 1) going from the turning point TP1 to the bifurcation PB; hence, the branches lying below the turning point TP1 are unstable, including the turning point TP2 as anticipated.

Let us now understand the meaning of these two instabilities, having in mind that they affect the subspace corresponding to the (noninjected) mode $H_y(\mathbf{r})$, which is off. The existence of an instability at the turning point TP1 is due to the fact that its corresponding injection intensity is null, that is, $\mathcal{I}_i^{\mathrm{TP1}} = 0$ (Fig. 1). In the absence of injection the system is rotationally symmetric in the transverse plane, and the 2DOPO can generate equally both modes $H_x(\mathbf{r})$ and $H_y(\mathbf{r})$; hence, at $\mathcal{I}_i = 0$ the solution with $\beta_y = 0$ is marginally unstable. On the other hand, the instability at PB is of a different nature as for injection intensities $\mathcal{I}_i > \mathcal{I}_i^{\mathrm{PB}}$ the one-mode solution is no more stable. As this instability governs the growth of mode $H_y(\mathbf{r})$ we conclude that at PB a pitchfork bifurcation takes place, giving rise to a new steady-state branch (the two-mode steady state; see Sec. III B). This instability is analogous to the one predicted in intracavity type-II second harmonic generation, where the field orthogonal (in the polarization sense) to the pumping one is generated at a pitchfork bifurcation [42–49]. We show in the remainder of the section that TP1 and PB are the only relevant instabilities in the 2DOPO-IS.

As for the second polynomial, it is, as commented, the one analyzed in [34]. We summarize next the results of that analysis and refer to [34] for the details. In particular, when $\sigma > 1$ an eigenvalue is null in correspondence with the turning point TP2 in Fig. 1, as usual, but this point (as well as the whole lower and intermediate branches) is already unstable, as stated above. On the other hand, a pair of complex-conjugate eigenvalues become purely imaginary (then with null real part) at an intensity $I_x = I_x^{\mathrm{HB1}}$ existing at any value of σ, thus signaling a so-called Hopf bifurcation. In the case $\sigma > 1$ the Hopf bifurcation is located on the upper branches in Fig. 1. It is then relevant to ask if this bifurcation can play a role in the 2DOPO-IS. The expression for I_x^{HB1} is not analytical in general; however, in the amplification regime $(\varphi_i = 0)$, $I_x^{\mathrm{HB1}} = 2(\kappa + \sigma + 1) > 2(\sigma + 1) = I_x^{\mathrm{PB}}$ [see (22)].

As $I_x^{\mathrm{HB1}} > I_x^{\mathrm{PB1}}$, the Hopf bifurcation is always preceded by the pitchfork bifurcation and then the former never comes into play. [Note that $I_x^{\mathrm{HB1}} \to I_x^{\mathrm{PB1}}$ for $\kappa \to 0$.] On the other hand, a second Hopf bifurcation (HB2) exists in the case $\sigma > 1$, but it is always located below the upper turning point TP1 in Fig. 1 [34] and then affects an already unstable solution. In other words, the Hopf bifurcations of the one-mode solution, which coincide with those of the 1DOPO-IS, are always preceded by other bifurcations genuine of the 2DOPO-IS, and then play no role in our case. This is a strong difference with the 1DOPO-IS [34] where the Hopf bifurcations can play a role. While we have not extended this analytical proof to arbitrary values of φ_{i}, we have convinced ourselves, through a numerical study, that its validity is general: The only bifurcations affecting the one-mode solution are the turning point bifurcation TP1 and the pitchfork bifurcation PB that gives rise to the switch on of the mode $H_y(\mathbf{r})$. In Fig. 2 we exemplify these results for two sets of parameters.

B. The two-mode solution

Next we consider the case $\beta_y \neq 0$, which is genuine of the present 2DOPO model. After simple but tricky algebra one finds $\beta_0 = -\exp(2i\varphi_{\mathrm{i}})$ (the intracavity pump intensity $|\beta_0|^2 = 1$ is quenched as usual in OPOs after a bifurcation is crossed),

$$\varphi_y = \varphi_{\mathrm{i}} \pm \frac{\pi}{2}, \quad \tan(\varphi_x - \varphi_{\mathrm{i}}) = -\frac{4\sigma}{\mathcal{I}_{\mathrm{i}}} \sin(2\varphi_{\mathrm{i}}), \tag{24}$$

with the constraint $(\varphi_x - \varphi_{\mathrm{i}}) \in [-\frac{\pi}{2}, \frac{\pi}{2}]$, and

$$I_x = \frac{\mathcal{I}_{\mathrm{i}}}{4} + \frac{4\sigma^2}{\mathcal{I}_{\mathrm{i}}} \sin^2 2\varphi_{\mathrm{i}}, \tag{25a}$$

$$I_y = \frac{\mathcal{I}_{\mathrm{i}}}{4} - \frac{4\sigma^2}{\mathcal{I}_{\mathrm{i}}} \sin^2 2\varphi_{\mathrm{i}} - 2[1 + \sigma \cos 2\varphi_{\mathrm{i}}]. \tag{25b}$$

Note that the phase of the mode $H_y(\mathbf{r})$, φ_y, can take any of two opposite values (this residual discrete symmetry survives even with the injection of the TEM_{10} mode) [see (24)]; in other words, the sign of β_y can be either, as usual in DOPOs above threshold.

For this solution to exist I_y must be a positive real [$I_x > 0$ always, see (25a)]. From (25b) the condition $I_y > 0$ is seen to be equivalent to $I_x > I_x^{\mathrm{PB}}$ or, alternatively, $\mathcal{I}_{\mathrm{i}} > \mathcal{I}_{\mathrm{i}}^{\mathrm{PB}}$, as expected: at the pitchfork bifurcation the two-mode solution is born.

In Fig. 3 we show the dependence on φ_{i} of $\mathcal{I}_{\mathrm{i}}^{\mathrm{PB}}$ for several values of σ. In the absence of pump, ($\sigma = 0$) $\mathcal{I}_{\mathrm{i}}^{\mathrm{PB}}$ is independent of the injection's phase φ_{i} as no reference phase exists in this case. For $\sigma \neq 0$ the threshold has a maximum in the case of amplification ($\varphi_{\mathrm{i}} = 0$) and a minimum in the case of attenuation ($\varphi_{\mathrm{i}} = \pi/2$). Interestingly, this minimum is zero when pumping is above the 2DOPO threshold ($\sigma > 1$). These results are actually quite intuitive: In the attenuation case, $\varphi_{\mathrm{i}} = \pi/2$, the injected mode $H_x(\mathbf{r})$ is depleted as it has the "wrong" phase, a fact that makes easier the amplification of the orthogonal mode $H_y(\mathbf{r})$, while the amplification case $\varphi_{\mathrm{i}} = 0$ is obviously detrimental for mode $H_y(\mathbf{r})$ as mode $H_x(\mathbf{r})$ is being amplified.

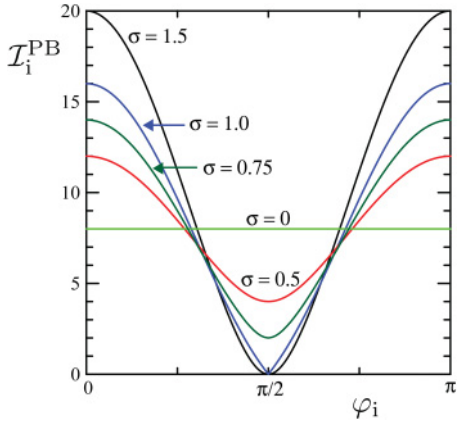

FIG. 3. (Color online) $\mathcal{I}_{\mathrm{i}}^{\mathrm{PB}}$ as a function of the injected field phase φ for the indicated values of σ. Above this value of the injected intensity the noninjected TEM_{01} mode is switched on. Note that for $\sigma > 1$ and $\varphi = \pi/2$ there is no threshold for the generation of the TEM_{01} mode.

This two-mode solution does not correspond to a HG mode as it consists of the superposition of two orthogonal HG modes with different amplitudes and phases. Curiously, in the special case $\varphi_{\mathrm{i}} = \pi/2$ and $\sigma = 1$, Eqs. (III B) imply that $\beta_x = \pm i\beta_y$, with $\beta_x = \frac{1}{2}\sqrt{\mathcal{I}_{\mathrm{i}}} e^{i\varphi_{\mathrm{i}}}$. This is also true for any φ_{i} value for sufficiently strong injection $\mathcal{I}_{\mathrm{i}}$. This means that in these cases the emitted mode is a pure LG mode with $+1$ or -1 OAM [see Eqs. (4)], which is a somewhat unexpected result.

As for the linear stability analysis of this two-mode solution one gets a sixth-order characteristic polynomial for the eigenvalue λ from which no conclusions can be drawn in general. However, in the special cases $\varphi_{\mathrm{i}} = 0$ and $\varphi_{\mathrm{i}} = \pi/2$ the polynomial gets factorized, giving rise to two cubic equations of the form $0 = P_{1,2}(\lambda)$, with

$$P_1(\lambda) = \lambda^3 + (\kappa + 2)\lambda^2 + \frac{\kappa}{2}(\mathcal{I}_{\mathrm{i}} \mp 4\sigma)\lambda + \frac{\kappa}{2}\mathcal{I}_{\mathrm{i}}, \tag{26}$$

and $P_2(\lambda) = P_1(\lambda) \mp 4\kappa(\sigma + 1)$, where the upper (lower) signs of the polynomials correspond to the case $\varphi_{\mathrm{i}} = 0$ ($\varphi_{\mathrm{i}} = \pi/2$). It is now easy to demonstrate that all eigenvalues have a negative real part when $\mathcal{I}_{\mathrm{i}} > \mathcal{I}_{\mathrm{i}}^{\mathrm{PB}}$: By taking $\lambda = i\Omega$ in the above polynomials one obtains the frequency at the bifurcations (if any) and the values of the injected signal strength $\mathcal{I}_{\mathrm{i}}$ leading to instabilities. It is easy to see that these bifurcations occur for $\mathcal{I}_{\mathrm{i}} < \mathcal{I}_{\mathrm{i}}^{\mathrm{PB}}$ (where the solution does not exist), and hence the two-mode solution is stable within its whole domain of existence. Through a numerical study of the characteristic polynomials for arbitrary injection phase φ_{i} we have convinced ourselves that this conclusion holds always.

C. Summary

In order to have a global picture of the steady states and their stability, which is necessary in order to perform the quantum analysis, we summarize the general results obtained up to now. After all, the picture is very simple.

On one hand, the one-mode solution [with mode $H_y(\mathbf{r})$ off] is stable from the null injection point $\mathcal{I}_{\mathrm{i}} = 0$ till the pitchfork bifurcation point at $\mathcal{I}_{\mathrm{i}} = \mathcal{I}_{\mathrm{i}}^{\mathrm{PB}}$. For $\sigma < 1$ this comprises the single branch existing between these points (Fig. 1), while for

$\sigma > 1$ the stable domain extends from the turning point TP1 along the upper branch till the pitchfork bifurcation point PB (Fig. 1). No other instabilities affect this solution. On the other hand, the two-mode solution is born at the pitchfork bifurcation point $\mathcal{I}_{\rm i} = \mathcal{I}_{\rm i}^{\rm PB}$ and is stable for any injection intensity $\mathcal{I}_{\rm i} > \mathcal{I}_{\rm i}^{\rm PB}$.

IV. QUANTUM SQUEEZING PROPERTIES

In this section we study the squeezing properties of the system. We define a general quadrature corresponding to mode $m = 0,x,y$ as

$$\hat{X}_m^\theta = e^{-i\theta}\hat{a}_m + e^{i\theta}\hat{a}_m^\dagger, \tag{27}$$

where θ is an arbitrary phase. What is measured in a typical squeezing (balanced homodyne detection) experiment is the *noise spectrum* of this quadrature out of the cavity, $V^{\rm out}(\omega;\hat{X}_m^\theta)$, where ω is the so-called *noise frequency* (not an optical frequency). This noise spectrum can be computed as

$$V^{\rm out}\big(\omega;\hat{X}_m^\theta\big) = 1 + S_m^\theta(\omega), \tag{28}$$

where the 1 marks the shot noise level, and the squeezing spectrum $S_m^\theta(\omega)$ is given, in the positive P representation (see [22] for details), by

$$S_m^\theta(\omega) = \frac{2}{g^2}(\kappa\delta_{m,0} + \delta_{m,x} + \delta_{m,y}) \times \int_{-\infty}^{+\infty} d\tau' \left\langle \delta x_m^\theta(\tau)\delta x_m^\theta(\tau+\tau')\right\rangle_P e^{-i\omega\tau'}, \tag{29}$$

where $\delta x_m^\theta = x_m^\theta - \langle x_m^\theta\rangle_P$, $\langle\cdot\rangle_P$ is a stochastic average following the Langevin equations (15), and

$$x_m^\theta = e^{-i\theta}\beta_m + e^{i\theta}\beta_m^+ \tag{30}$$

is a "normalized quadrature" [see (27)]. In order to arrive at (29) we have taken into account the normalizations (12) and the definitions (14) (see [22]).

For coherent (or vacuum) fields $V^{\rm out}(\omega;\hat{X}_m^\theta) = 1$ for all ω (standard quantum limit), while if $V^{\rm out}(\omega;\hat{X}_m^\theta) < 1$ for some ω the considered field quadrature is said to be squeezed (displays less fluctuations than the vacuum). Finally $V^{\rm out}(\omega;\hat{X}_m^\theta) = 0$ denotes the complete absence of fluctuations (perfect squeezing) in quadrature $\hat{X}_m^\theta$ at noise frequency ω.

In the following we concentrate on the quantum fluctuations of mode $H_y(\mathbf{r})$, which is genuine of the model we are studying, and we do it below its generation threshold, that is, when the classical steady state is the one-mode solution. This is the more interesting case as nice squeezing properties are expected at bifurcation points and we have seen that the only bifurcations affecting the one-mode solution are those associated with field $H_y(\mathbf{r})$. Fluctuations in other variables can be studied following the next lines, although none of them exhibit outstanding features. Hence, we consider in the following the noise spectrum $V^{\rm out}(\omega;\hat{X}_y^\theta) = 1 + S_y^\theta(\omega)$, with

$$S_y^\theta(\omega) = \frac{2}{g^2}\int_{-\infty}^{+\infty} d\tau' \left\langle \delta x_y^\theta(\tau)\delta x_y^\theta(\tau+\tau')\right\rangle_P e^{-i\omega\tau'}. \tag{31}$$

A. The linearized quantum equations in the case of the one-mode solution

As the noise-coupling parameter g in Eqs. (13) is tiny ($g \sim 10^{-6}$ under typical experimental conditions [22]), fluctuations around the steady states will be small and a linearized treatment is in order (see, however, [26,27] for remarks). Accordingly, we write $\beta_m = \bar{\beta}_m + b_m$, where the overbar indicates steady state and b_m is a small fluctuation. Then Eqs. (13) can be written, after linearizing in the b's and considering the one-mode solution ($\bar{\beta}_y = 0$), as

$$\dot{\mathbf{b}}_{0x} = \mathcal{L}_{0x}\mathbf{b}_{0x} + g\sqrt{I_0}\zeta_{0x}(t), \tag{32a}$$

$$\dot{\mathbf{b}}_y = \mathcal{L}_y\mathbf{b}_y + g\sqrt{I_0}\zeta_y(t), \tag{32b}$$

where $\mathbf{b}_{0x} = \mathrm{col}(b_0,b_0^+,b_x,b_x^+)$, $\mathbf{b}_y = \mathrm{col}(b_y,b_y^+)$,

$$\mathcal{L}_{0x} = \begin{pmatrix} -\kappa & 0 & -\kappa\bar{\beta}_x & 0 \\ 0 & -\kappa & 0 & -\kappa\bar{\beta}_x^* \\ \bar{\beta}_x^* & 0 & -1 & \bar{\beta}_0 \\ 0 & \bar{\beta}_x & \bar{\beta}_0^* & -1 \end{pmatrix}, \tag{33a}$$

$$\mathcal{L}_y = \begin{pmatrix} -1 & \bar{\beta}_0 \\ \bar{\beta}_0^* & -1 \end{pmatrix}, \tag{33b}$$

and the noise vectors read

$$\zeta_{0x} = \mathrm{col}\big(0,0,e^{i\varphi_0/2}\zeta_x,e^{-i\varphi_0/2}\zeta_x^+\big), \tag{34a}$$

$$\zeta_y = \mathrm{col}\big(e^{i\varphi_0/2}\zeta_y,e^{-i\varphi_0/2}\zeta_y^+\big). \tag{34b}$$

The procedure we follow below is the same we have used elsewhere [17,21,22,28,29]: We project quantum fluctuations onto the eigenvectors of matrix $\mathcal{L}_y$, as these projections are, up to a constant factor, the relevant quadratures of the output modes (those that are maximally squeezed or antisqueezed).

B. Squeezing properties of the one-mode solution

The eigensystem of matrix $\mathcal{L}_y$ ($\mathcal{L}_y\cdot\mathbf{w}_i = \lambda_i\mathbf{w}_i$) comprises the eigenvalues $\lambda_{1,2}$ given in (21) and the associated eigenvectors

$$\mathbf{w}_{1,2} = (e^{i\varphi_0/2}, \mp e^{-i\varphi_0/2})/\sqrt{2}, \tag{35}$$

with φ_0 given by Eq. (19b). Defining the projections $c_y^{(j)} = \mathbf{w}_j^*\cdot\mathbf{b}_y$, we obtain the following decoupled equations:

$$\dot{c}_y^{(j)} = \lambda_j c_y^{(j)} + g\sqrt{I_0}\zeta_y^{(j)}(t), \tag{36}$$

where we defined the standard real white Gaussian noises $\zeta_y^{(1,2)} = (\zeta_y \mp \zeta_y^+)/\sqrt{2}$. It is then trivial to obtain [see (30)]

$$x_y^{\varphi_0/2} = \sqrt{2}c_y^{(2)}, \quad x_y^{\varphi_0/2+\pi/2} = -i\sqrt{2}c_y^{(1)}. \tag{37}$$

After integration of (36) and substitution into (31) (see [22] for details), we obtain

$$V^{\rm out}\big(\omega;\hat{X}_y^{\varphi_0/2}\big) = 1 + \frac{4\sqrt{I_0}}{(1-\sqrt{I_0})^2+\omega^2}, \tag{38a}$$

$$V^{\rm out}\big(\omega;\hat{X}_y^{\varphi_0/2+\pi/2}\big) = 1 - \frac{4\sqrt{I_0}}{(1+\sqrt{I_0})^2+\omega^2}. \tag{38b}$$

The only quadrature that can be perfectly squeezed ($V^{\rm out}$=0) is $X_y^{\varphi_0/2+\pi/2}$ at $\omega = 0$ when $I_0 = 1$ (quadrature $X_y^{\varphi_0/2}$ exhibits antisqueezing). According to (19) and (17), this

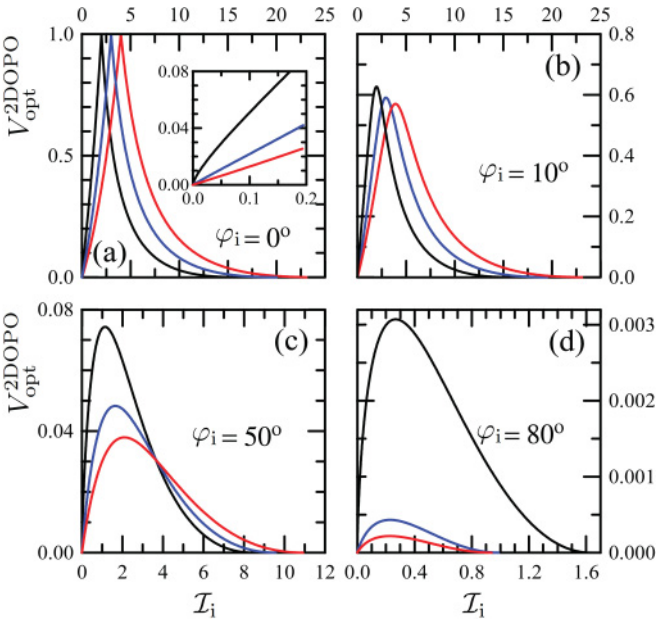

FIG. 4. (Color online) Dependence of the optimal noise spectrum V_{opt}^{2DOPO} [Eq. (38b)] on the injected intensity $\mathcal{I}_i$ for the four values of the injection phase φ_i indicated in each figure. For each of φ_i, three values of σ have been plotted, namely, $\sigma = 1$ (black), 1.5 (blue), and 2 (red), which correspond to the upper, middle, and lower curves at the left of the maxima, respectively. Notice the different scales in each figure.

happens only in two cases: either at the turning point TP1 ($\mathcal{I}_i = 0$, no injection, where there exists perfect squeezing because of the rotational symmetry breaking occurring in the 2DOPO [21,22] at any $\sigma > 1$), or when $\mathcal{I}_i = \mathcal{I}_i^{PB}$, which corresponds to the pitchfork bifurcation where mode $H_y(\mathbf{r})$ is switched on. Figure 4 shows the dependence on the injected intensity $\mathcal{I}_i$ of the optimal squeezing level $V_{opt}^{2DOPO} \equiv V^{out}(\omega = 0; \hat{X}_y^{\varphi_0/2+\pi/2})$ [see Eq. (38b)] for several values of the pump level σ and the injection phase φ_i.

In terms of the injection's external power [see (16), (14), and the Appendix], the injection intensity parameter $\mathcal{I}_i$ reads

$$\mathcal{I}_i = \frac{\chi^2 |\mathcal{E}_s|^2}{\gamma_s^3 \gamma_p} = 2\frac{P_s}{P_{p,thr}}, \tag{39}$$

where $P_{p,thr}$ is the usual DOPO threshold pump power, that is, the pump power needed for making the signal field oscillate when no injection is used ($\mathcal{I}_i = 0$), which can be found from (A3) with $|\mathcal{E}_{p,thr}|^2 = (\gamma_s \gamma_p/\chi)^2$ as follows from the threshold condition $\sigma = 1$; P_s is the actual injection power. In usual experiments, where the injected seed is used for active locking purposes, P_s is a small fraction of the pump power P_p (say 0.001–0.1) and that is the reason why we show a zoom of the region $\mathcal{I}_i \in [0,0.2]$ in Fig. 4(a) (the enlargement is representative of what happens in the rest of cases represented in Fig. 4). It is remarkable the very small squeezing degradation that the injected field induces in the 2DOPO-IS model, specially close to attenuation ($\varphi_i = \pi/2$).

A relevant issue is how this squeezing level compares with the usual 1DOPO-IS [50]. This is shown in Fig. 5, where we represent the optimal squeezing level in both cases. That of the 1DOPO-IS, V_{opt}^{1DOPO}, is shown in the limit $\kappa \to \infty$,

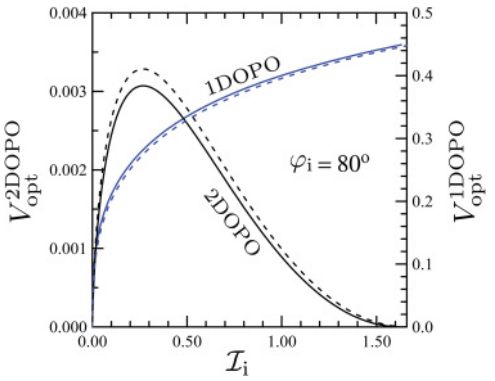

FIG. 5. (Color online) Comparison between the optimum squeezing levels of the 2DOPO-IS, V_{opt}^{2DOPO} (black lines, left vertical axis), and that of the 1DOPO-IS [50], V_{opt}^{1DOPO} (blue lines, right vertical axis), as a function of the injected intensity $\mathcal{I}_i$. We took $\varphi_i = 80^o$ and two values of σ: $\sigma = 1$ (solid lines) and $\sigma = 0.99$ (dashed lines).

which is a common limit from the experimental viewpoint and yields its best noise reduction (the 2DOPO-IS level, V_{opt}^{2DOPO}, does not depend on κ). As compared with the usual 1DOPO-IS we observe that the squeezing level of the 2DOPO-IS is quite insensitive on the injection (note the different scales for both quantities). As well as that, by increasing $\mathcal{I}_i$ from zero, the squeezing first degrades but, in the 2DOPO-IS, it improves again unlike the 1DOPO-IS case. We want to stress that the squeezing level in a 1DOPO-IS is highly sensitive to the pumping level σ (only very close to $\sigma = 1$ the squeezing is high), while in the case of the 2DOPO-IS large squeezing levels can be found for any σ. This phenomenon is directly related to the rotational symmetry breaking which is the origin of the perfect, noncritical squeezing occurring for any $\sigma > 1$ for null injection. We can conclude that adding a small injection to a 2DOPO could be useful to improve the levels of squeezing available with 1DOPOs.

V. CONCLUSIONS

We have studied a 2DOPO with an injected TEM_{10} mode at the signal frequency. The main motivation for this study was to determine up to what extent a smooth breaking of the rotational symmetry of the system could help in the observation of the phenomenon of squeezing due to spontaneous rotational symmetry breaking [21,22]. We have shown that the injection degrades the squeezing level of the TEM_{01} mode only slightly in a wide parameter region, as for some injection threshold a new bifurcation leading to the generation of this noninjected mode appears in the system. Moreover, we have shown that the noise reduction performance of this system improves that of the single-mode DOPO with injected signal [34,41].

ACKNOWLEDGMENTS

We acknowledge fruitful discussions with Claude Fabre and Nicolas Treps. This work has been supported by the Spanish Government and the European Union FEDER through Project No. FIS2008-06024-C03-01. C.N.-B. is a grant holder of the FPU program of the Ministerio de Ciencia e Innovación (Spain).

APPENDIX A: THE INJECTION PARAMETERS

Here we relate the injection model parameters $\mathcal{E}_{\rm p}$ and $\mathcal{E}_{\rm s}$ to physical parameters. According to Eqs. (10) $\mathcal{E}_{\rm p}$ and $\mathcal{E}_{\rm s}$ are proportional to the intracavity fields α_0 and α_x when the interaction is switched off ($\chi = 0$), in which case the equations become $\dot{\alpha}_m = \mathcal{E}_m - \gamma_m \alpha_m$, whose long time solution is $\alpha_m = \mathcal{E}_m/\gamma_m$. This intracavity field amplitude corresponds to an actual electric field given by (5), (6a), and (6b), that is,

$$E_m = i\sqrt{\frac{\hbar\omega_m}{\varepsilon_0 nL}}\frac{\mathcal{E}_m}{\gamma_m}M_m(\mathbf{r})e^{-i\omega_m t} + \text{c.c.}, \tag{A1}$$

where $M_m(\mathbf{r})$ represents the mode shape [$G(\mathbf{r})$ for $m = 0$, or $H_{x,y}(\mathbf{r})$ for $m = x, y$]. This intracavity field is the consequence of the injection of an external field that, in terms of its power P_m, can be written as

$$E_m^{\rm ext} = i\sqrt{\frac{P_m}{2\varepsilon_0 c}}M_m(\mathbf{r})e^{-i\omega_m t} + \text{c.c.} \tag{A2}$$

On the other hand, the intracavity field due to $E_m^{\rm ext}$ is easily computed as $E_m = \frac{t_m}{1-r_m}E_m^{\rm ext}$ (interferometer relation), where t_m and $r_m = \sqrt{1-t_m^2}$ are the (Fresnel) transmission and reflection coefficients of the (assumed) unique coupling mirror, respectively. As the latter expression for E_m and (A1) must coincide by definition, this fixes a relation between the parameter $\mathcal{E}_m$ and the actual external injected power P_m. In the limit $t_m^2 \to 0$ (low-transmission coupling mirror, implicitly assumed in all the theory), one finds

$$|\mathcal{E}_m|^2 = \frac{n\gamma_m}{\hbar\omega_m}P_m, \tag{A3}$$

where $\gamma_m = ct_m^2/2L$.

APPENDIX B: INFLUENCE OF OTHER MODES

In this appendix we analyze the classical solutions to a general 2DOPO-IS when all cavity modes are considered as possibly excited by the parametric interaction. Our goal is to show that, as long as the $H_{x,y}(\mathbf{r})$ frequency-degenerate modes are the ones with the lowest threshold, no other mode will oscillate when injecting the $H_x(\mathbf{r})$ mode considered in this article.

Then, apart from the modes $G_0(\mathbf{r})$ and $H_{x,y}(\mathbf{r})$ we have considered so far, we consider here as well all the LG modes $L_q(\mathbf{r})$ around the injected frequency ω_0, characterized by a multi-index q containing the longitudinal (principal) index, a radial index, and an OAM index. The Hamiltonian in this case is a straightforward extension of (9), namely,

$$\hat{H} = i\hbar\Big[\mathcal{E}_{\rm p}\hat{a}_0^\dagger + \mathcal{E}_{\rm s}\hat{a}_x^\dagger + \tfrac{1}{2}\chi a_0\big(\hat{a}_x^{\dagger 2} + \hat{a}_y^{\dagger 2}\big) \tag{B1}$$

$$+ \sum_q \chi_q a_0 \hat{a}_q^\dagger \hat{a}_{\widetilde{q}}^\dagger\Big] + \text{H.c.}, \tag{B2}$$

where $\hat{a}_q^\dagger$ represents the boson creation operator of the LG cavity mode $L_q(\mathbf{r})$, and the subscript $\widetilde{q}$ denotes the mode complementary to that one in the sense that the down-conversion terms $a_0\hat{a}_q^\dagger\hat{a}_{\widetilde{q}}^\dagger$ conserve both energy and OAM. We use the LG basis for these extra modes (instead of the HG basis we use for the injected mode family) for the sake of simplicity. Note that we have ignored detunings for these extra modes (that actually would be detrimental for their switch on). The rest of symbols keep their meanings.

The classical dynamic equations corresponding to (B1) read

$$\dot{\alpha}_0 = \mathcal{E}_{\rm p} - \gamma_{\rm p}\alpha_0 - \tfrac{1}{2}\chi\big(\alpha_x^2 + \alpha_y^2\big) - \textstyle\sum_q \chi_q \alpha_q \alpha_{\widetilde{q}} \tag{B3a}$$

$$\dot{\alpha}_x = \mathcal{E}_{\rm s} - \gamma_{\rm s}\alpha_x + \chi\alpha_0\alpha_x^*, \tag{B3b}$$

$$\dot{\alpha}_y = -\gamma_{\rm s}\alpha_y + \chi\alpha_0\alpha_y^*, \tag{B3c}$$

$$\dot{\alpha}_q = -\gamma_q\alpha_q + \chi_q\alpha_0\alpha_{\widetilde{q}}^*, \tag{B3d}$$

$$\dot{\alpha}_{\widetilde{q}} = -\gamma_{\widetilde{q}}\alpha_{\widetilde{q}} + \chi_q\alpha_0\alpha_q^*. \tag{B3e}$$

Let us first analyze the noninjected ($\mathcal{E}_{\rm s} = 0$) OPO threshold. A straightforward linear stability analysis of the steady-state solution where all subharmonic modes are off shows that the threshold for modes $H_{x,y}(\mathbf{r})$ occurs at $\mathcal{E}_{\rm p} = \gamma_{\rm p}\gamma_{\rm s}/\chi \equiv \mathcal{E}^{\rm th}$, while that for the couple $L_q(\mathbf{r})$–$L_{\widetilde{q}}(\mathbf{r})$ occurs at $\mathcal{E}_{\rm p} = \gamma_{\rm p}\sqrt{\gamma_q\gamma_{\widetilde{q}}}/\chi_q \equiv \mathcal{E}_q^{\rm th}$. In this paper we assume that the OPO configuration is such that the first threshold is the lowest one, that is,

$$\mathcal{E}^{\rm th} < \mathcal{E}_q^{\rm th}. \tag{B4}$$

In this free-running OPO configuration the situation is simple: Once the external pump amplitude $\mathcal{E}_{\rm p}$ crosses the lowest threshold $\mathcal{E}^{\rm th}$, the corresponding pair of modes starts oscillating and the intracavity pump amplitude α_0 gets frozen at its threshold value $\alpha_0 = \gamma_{\rm s}/\chi$. As this quantity is the one that governs the stability of any other couple of modes, the rest of the (nonoscillating) modes are off forever; this was explicitly proved in [17].

Our concern is whether some couple of modes $L_q(\mathbf{r})$–$L_{\widetilde{q}}(\mathbf{r})$ can start oscillating when signal injection is considered, which would invalidate our previous analysis. The question is pertinent as, unlike the free-running OPO, when introducing injection at the subharmonic the intracavity pump amplitude α_0 is only constant above the pitchfork bifurcation studied in Sec. III. The question can be set in mathematical terms by considering Eqs. (B3) linearized around the solution in which all the modes are off except the injected one $H_x(\mathbf{r})$ (and the pump mode, obviously).

Under these conditions, the equations for the $H_y(\mathbf{r})$ mode are decoupled from the rest of the modes. In particular, defining the vector $\mathbf{y} = \text{col}(\alpha_y, \alpha_y^*)$, these can be written as the linear system $\dot{\mathbf{y}} = \mathcal{L}_y\mathbf{y}$, with

$$\mathcal{L}_y = \begin{bmatrix} -\gamma_{\rm s} & \chi\bar{\alpha}_0 \\ \chi\bar{\alpha}_0^* & -\gamma_{\rm s} \end{bmatrix}, \tag{B5}$$

where $\bar{\alpha}_0$ is the steady-state value of the intracavity pump amplitude. The solution of this linear system has the form $\mathbf{y}(t) = c_+e^{\lambda_+ t}\mathbf{v}_+ + c_-e^{\lambda_- t}\mathbf{v}_-$, where $\lambda_\pm$ are eigenvalues of $\mathcal{L}_y$ and $\mathbf{v}_\pm$ are their associated eigenvectors. Simple algebra leads to $\lambda_\pm = -2\gamma_{\rm s} \pm 2\chi|\bar{\alpha}_0|$. As long as $\lambda_\pm < 0$, the fluctuations of the mode $H_y(\mathbf{r})$ are damped, and therefore this mode remains off. The $\lambda_+ = 0$ point leads then to the instability by which the mode $H_y(\mathbf{r})$ is switched on, as for $\lambda_+ > 0$ its fluctuations tend to grow, eventually leading to a nonzero value of α_y in the steady state. This point is reached when the intracavity pump amplitude arrives to the value $|\bar{\alpha}_0| = \gamma_{\rm s}/\chi$, or in terms of the

normalized variables β_j [see (12)], $|\bar{\beta}_0| = 1$. Note that this point coincides with the pitchfork bifurcation we have already studied. Note also that once the $H_y(\mathbf{r})$ mode is switched on, Eq. (B3c) forces the pump amplitude to freeze at the $|\bar{\beta}_0| = 1$ value, irrespective of how much we increase the external injections $\mathcal{E}_p$ and $\mathcal{E}_s$.

On the other hand, upon defining $\mathbf{q} = \mathrm{col}(\alpha_q, \alpha^*_{\tilde{q}})$, the linearized versions of Eqs. (B3d) and (B3e) can be recast as the linear system $\dot{\mathbf{q}} = \mathcal{L}_q \mathbf{q}$, where

$$\mathcal{L}_q = \begin{bmatrix} -\gamma_q & \chi_q \bar{\alpha}_0 \\ \chi_q \bar{\alpha}^*_0 & -\gamma_{\tilde{q}} \end{bmatrix}, \tag{B6}$$

whose solution is again of the form $\mathbf{q}(t) = b_+ e^{\nu_+ t}\mathbf{w}_+ + b_- e^{\nu_- t}\mathbf{w}_-$, $\nu_\pm$ and $\mathbf{w}_\pm$ being the eigenvalues and eigenvectors of $\mathcal{L}_q$, respectively. Simple algebra leads to $\nu_\pm = -(\gamma_q + \gamma_{\tilde{q}}) \pm \sqrt{(\gamma_q - \gamma_{\tilde{q}})^2 + 4\chi_q^2 |\bar{\alpha}_0|^2}$; similar to the analysis of the $H_y(\mathbf{r})$ mode, the instability leading to the switching on of the modes $L_q(\mathbf{r})$–$L_{\tilde{q}}(\mathbf{r})$ is reached at $\nu_+ = 0$, or alternatively when the pump amplitude reaches the value $|\bar{\alpha}_0| = \sqrt{\gamma_q \gamma_{\tilde{q}}}/\chi_q$. In terms of the scaled amplitude β_0 (12) and the thresholds, this condition can be rewritten as $|\bar{\beta}_0| = \mathcal{E}_q^{\mathrm{th}}/\mathcal{E}^{\mathrm{th}} > 1$ [see (B4)], which can never be satisfied because once the intracavity pump amplitude reaches the value $|\bar{\beta}_0| = 1$, the $H_y(\mathbf{r})$ mode starts oscillating, and β_0 gets frozen to that value, as already discussed. Hence, $|\bar{\beta}_0| = 1$ is an upper bound to the intracavity pump amplitude, which means that $\nu_\pm < 0$ is always satisfied and the pairs $L_q(\mathbf{r})$–$L_{\tilde{q}}(\mathbf{r})$ can never be excited.

We therefore conclude that the three-mode model we have worked with is correct as long as the OPO is designed in such a way that $H_{x,y}(\mathbf{r})$ are the lowest threshold modes.

[1] L. A. Wu, H. J. Kimble, J. L. Hall, and H. Wu, Phys. Rev. Lett. **57**, 2520 (1986).

[2] Y. Takeno, M. Yukawa, H. Yonezawa, and A. Furusawa, Opt. Express **15**, 4321 (2007).

[3] H. Vahlbruch, M. Mehmet, S. Chelkowski, B. Hage, A. Franzen, N. Lastzka, S. Gossler, K. Danzmann, and R. Schnabel, Phys. Rev. Lett. **100**, 033602 (2008).

[4] M. Mehmet, H. Vahlbruch, N. Lastzka, K. Danzmann, and R. Schnabel, Phys. Rev. A **81**, 013814 (2010).

[5] A. Heidmann, R. J. Horowicz, S. Reynaud, E. Giacobino, C. Fabre, and G. Camy, Phys. Rev. Lett. **59**, 2555 (1987).

[6] Z. Y. Ou, S. F. Pereira, H. J. Kimble, and K. C. Peng, Phys. Rev. Lett. **68**, 3663 (1992).

[7] S. L. Braunstein and P. van Loock, Rev. Mod. Phys. **77**, 513 (2005)

[8] U. L. Andersen, G. Leuchs, and C. Silberhorn, Laser Photon. Rev. **4**, 337 (2010).

[9] N. Treps, U. Andersen, B. Buchler, P. K. Lam, A. Mâitre, H-A. Bachor, and C. Fabre, Phys. Rev. Lett. **88**, 203601 (2002).

[10] N. Treps, N. Grosse, W. P. Bowen, C. Fabre, H-A. Bachor, and P. K. Lam, Science **301**, 940 (2003).

[11] B. Lamine, C. Fabre, and N. Treps, Phys. Rev. Lett. **101**, 123601 (2008).

[12] A. Furusawa, J. L. Sørensen, S. L. Braunstein, C. A. Fuchs, H. J. Kimble, and E. S. Polzik, Science **282**, 706 (1998).

[13] P. van Loock and S. L. Braunstein, Phys. Rev. Lett. **84**, 3482 (2000).

[14] T. Aoki, N. Takei, H. Yonezawa, K. Wakui, T. Hiraoka, A. Furusawa, and P. van Loock, Phys. Rev. Lett. **91**, 080404 (2003).

[15] G. J. de Valcárcel, G. Patera, N. Treps, and C. Fabre, Phys. Rev. A **74**, 061801 (2006).

[16] G. Patera, N. Treps, C. Fabre, and G. J. de Valcárcel, Eur. Phys. J. D **56**, 123 (2010).

[17] C. Navarrete-Benlloch, G. J. de Valcárcel, and E. Roldán, Phys. Rev. A **79**, 043820 (2009).

[18] M. Lassen, G. Leuchs, and U. L. Andersen, Phys. Rev. Lett. **102**, 163602 (2009).

[19] J. Janousek, K. Wagner, J-F. Morizur, N. Treps, P. K. Lam, C. C. Harb, and H-A. Bachor, Nat. Photon. **3**, 399 (2009).

[20] B. Chalopin, F. Scazza, C. Fabre, and N. Treps, Phys. Rev. A **81**, 061804(R) (2010).

[21] C. Navarrete-Benlloch, E. Roldán, and G. J. de Valcárcel, Phys. Rev. Lett. **100**, 203601 (2008).

[22] C. Navarrete-Benlloch, A. Romanelli, E. Roldán, and G. J. de Valcárcel, Phys. Rev. A **81**, 043829 (2010).

[23] B. Coutinho dos Santos, K. Dechoum, and A. Z. Khoury, Phys. Rev. Lett. **103**, 230503 (2009).

[24] B. Yurke, Phys. Rev. A **29**, 408 (1984).

[25] M. J. Collett and C. W. Gardiner, Phys. Rev. A **30**, 1386 (1984).

[26] S. Chaturvedi, K. Dechoum, and P. D. Drummond, Phys. Rev. A **65**, 033805 (2002).

[27] P. D. Drummond, K. Dechoum, and S. Chaturvedi, Phys. Rev. A **65**, 033806 (2002).

[28] I. Pérez-Arjona, E. Roldán, and G. J. de Valcárcel, Europhys. Lett. **74**, 247 (2006).

[29] I. Pérez-Arjona, E. Roldán, and G. J. de Valcárcel, Phys. Rev. A **75**, 063802 (2007).

[30] F. V. García-Ferrer, C. Navarrete-Benlloch, G. J. de Valcárcel, and E. Roldán, IEEE J. Quantum Electron. **45**, 1404 (2010).

[31] F. V. García-Ferrer, C. Navarrete-Benlloch, G. J. de Valcárcel, and E. Roldán, Opt. Lett. **35**, 2194 (2010).

[32] G. J. de Valcárcel, F. V. Garcia-Ferrer, R. M. Höppner, I. Pérez-Arjona, C. Navarrete-Benlloch, and E. Roldán, Proc. SPIE **7727**, 772704 (2010).

[33] C. Navarrete-Benlloch and G. J. de Valcárcel (unpublished).

[34] I. E. Protsenko, L. A. Lugiato, and C. Fabre, Phys. Rev. A **50**, 1627 (1994).

[35] B. Coutinho dos Santos, K. Dechoum, A. Z. Khoury, L. F. da Silva, and M. K. Olsen, Phys. Rev. A **72**, 033820 (2005).

[36] B. Coutinho dos Santos, C. E. R. Souza, K. Dechoum, and A. Z. Khoury, Phys. Rev. A **76**, 053821 (2007).

[37] P. D. Drummond and C. W. Gardiner, J. Phys. A **13**, 2353 (1980).

[38] H. J. Carmichael, *Statistical Methods in Quantum Optics* Vol. 1 (Springer, Berlin, 1999).

[39] C. W. Gardiner and P. Zoller, *Quantum Noise* (Springer, Berlin, 2000).

[40] Equations (10) are equivalent in both Ito and Stratonovich interpretations [22], and we treat them in the latter sense because then the usual differential calculus holds. As we are using a positive P representation, quantum expectation values of normally ordered functions of boson operators equal stochastic averages, as given by Eqs. (10), of the same functions changing boson operators by the associated stochastic variables.

[41] P. D. Drummond, K. J. McNeil, and D. F. Walls, Opt. Commun. **28**, 255 (1979).

[42] Z. Y. Ou, Phys. Rev. A **49**, 4902 (1994).

[43] A. Eschmann and M. D. Reid, Phys. Rev. A **49**, 2881 (1994).

[44] M. W. Jack, M. J. Collett, and D. F. Walls, Phys. Rev. A **53**, 1801 (1996).

[45] U. L. Andersen and P. Buchhave, J. Opt. Soc. Am. B **20**, 1947 (2003).

[46] U. L. Andersen and P. Buchhave, J. Opt. B: Quantum Semiclass. Opt. **5**, S486 (2003).

[47] Z. Zhai, Y. Li, and J. Gao, Phys. Rev. A **69**, 044301 (2004).

[48] Z. Zhai, H. Zou, J. Zhang, and J. Gao, J. Opt. Soc. Am. B **22**, 878 (2005).

[49] Y. Luo, Y. Li, C. Xie, Q. Pan, and K. Peng, Opt. Lett. **30**, 1491 (2005).

[50] The optimal squeezing level in a 1DOPO IS is calculated in [34]. It is given by Eq. (187) in that paper with the following substitutions in order to adapt the expression to our notation: $\{A_0, A_1, \Delta_0, \Delta_1, E, e, \gamma,\} \to \{\beta_0, \beta_x/\sqrt{2}, 0, 0, \sigma, \varepsilon_i/\sqrt{2}, \kappa^{-1}\}$.